AGU PUBLICATIONS

Global Biogeochemical Cycles

RESEARCH ARTICLE

10.1002/2014GB004929

Key Points:
- Air-sea disequilibrium of carbon isotopes decreases with rising atmospheric CO_2
- The pCO_2 effect increased ^{14}C reservoir ages by 250 years during LGM
- High pCO_2 weakens oceanic ^{13}C gradients, relevant for past and future

Correspondence to:
E. Galbraith,
eric.galbraith@mcgill.ca

Citation:
Galbraith, E. D., E. Y. Kwon, D. Bianchi, M. P. Hain, and J. L. Sarmiento (2015), The impact of atmospheric pCO_2 on carbon isotope ratios of the atmosphere and ocean, *Global Biogeochem. Cycles*, *29*, 307–324, doi:10.1002/2014GB004929.

Received 1 JUL 2014
Accepted 4 FEB 2015
Accepted article online 9 FEB 2015
Published online 21 MAR 2015
Corrected 13 APR 2015

This article was corrected on 13 APR 2015. See the end of the full text for details.

The impact of atmospheric pCO_2 on carbon isotope ratios of the atmosphere and ocean

Eric D. Galbraith[1], Eun Young Kwon[2], Daniele Bianchi[1,3], Mathis P. Hain[4], and Jorge L. Sarmiento[5]

[1]Department of Earth and Planetary Sciences, McGill University, Montreal, Quebec, Canada, [2]School of Earth and Environmental Sciences (BK21), Seoul National University, Seoul, South Korea, [3]School of Oceanography, University of Washington, Seattle, Washington, USA, [4]National Oceanography Centre Southampton, University of Southampton, Southampton, UK, [5]AOS Program, Princeton University, Princeton, New Jersey, USA

Abstract It is well known that the equilibration timescale for the isotopic ratios $^{13}C/^{12}C$ and $^{14}C/^{12}C$ in the ocean mixed layer is on the order of a decade, 2 orders of magnitude slower than for oxygen. Less widely appreciated is the fact that the equilibration timescale is quite sensitive to the speciation of dissolved inorganic carbon (DIC) in the mixed layer, scaling linearly with the ratio DIC/CO_2, which varies inversely with atmospheric pCO_2. Although this effect is included in models that resolve the role of carbon speciation in air-sea exchange, its role is often unrecognized, and it is not commonly considered in the interpretation of carbon isotope observations. Here we use a global three-dimensional ocean model to estimate the redistribution of the carbon isotopic ratios between the atmosphere and ocean due solely to variations in atmospheric pCO_2. Under Last Glacial Maximum (LGM) pCO_2, atmospheric $\Delta^{14}C$ is increased by ≈30‰ due to the speciation change, all else being equal, raising the surface reservoir age by about 250 years throughout most of the ocean. For ^{13}C, enhanced surface disequilibrium under LGM pCO_2 causes the upper ocean, atmosphere, and North Atlantic Deep Water $\delta^{13}C$ to become at least 0.2‰ higher relative to deep waters ventilated by the Southern Ocean. Conversely, under high pCO_2, rapid equilibration greatly decreases isotopic disequilibrium. As a result, during geological periods of high pCO_2, vertical $\delta^{13}C$ gradients may have been greatly weakened as a direct chemical consequence of the high pCO_2, masquerading as very well ventilated or biologically dead Strangelove Oceans. The ongoing anthropogenic rise of pCO_2 is accelerating the equilibration of the carbon isotopes in the ocean, lowering atmospheric $\Delta^{14}C$ and weakening $\delta^{13}C$ gradients within the ocean to a degree that is similar to the traditional fossil fuel "Suess" effect.

1. Introduction

The distribution of carbon isotopes in the modern ocean, together with geological reconstructions of its past variability, has fundamentally shaped our understanding of ocean circulation and biological carbon cycling. Among the processes that control $^{13}C/^{12}C$ and $^{14}C/C$ (expressed as $\delta^{13}C$ and $\Delta^{14}C$, respectively, the latter following the conventions of *Stuiver and Polach* [1977]), this paper draws attention to a feature of the air-sea balance of carbon isotopes that is a straightforward consequence of carbon chemistry but is not widely recognized: the equilibration timescale of carbon isotopic ratios via air-sea exchange is quite sensitive to the speciation of dissolved inorganic carbon (DIC) in the surface ocean, which varies strongly with the atmospheric partial pressure of carbon dioxide, pCO_2. This direct consequence of carbon speciation is referred to here as the "pCO_2 effect." The effect, particularly on radiocarbon, has been noted in passing by many authors, including *Broecker and Peng* [1974], *Siegenthaler* [1986], *Follows and Marshall* [1996], *Stocker and Wright* [1996], *Bard* [1998], *Broecker and Barker* [2007], and *Butzin et al.* [2012], but without elaboration on the underlying mechanism or detailed exploration of its magnitude and global implications under a range of pCO_2.

The pCO_2 effect would be of little interest if the $\delta^{13}C$ and $\Delta^{14}C$ of the surface ocean were close to equilibrium with the atmosphere. However, both $\delta^{13}C$ and $\Delta^{14}C$ are far from equilibrium across most of the ocean surface, for different reasons, particularly in regions of deep water formation. For $\delta^{13}C$, disequilibrium is maintained by the rapid cooling of surface waters prior to sinking so that the $\delta^{13}C$ of newly formed deep waters is not equilibrated to their cold temperatures, and by the biological pump, which discriminates against ^{13}C in the production and transport of organic carbon to depth. Both forms of disequilibrium leave the deep ocean depleted in ^{13}C [*Schmittner et al.*, 2013]. For radiocarbon, it is radioactive decay that leaves

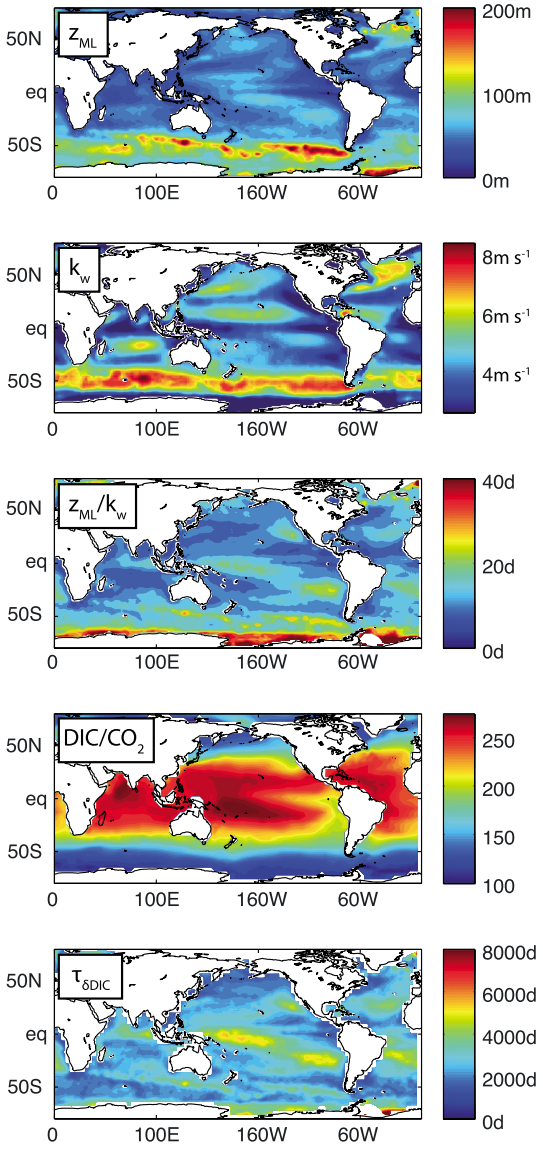

Figure 1. Determinants of the equilibration timescale of carbon isotopes at the ocean surface. (first row) Annually averaged mixed layer depth z_{ML} [*de Boyer Montegut et al.*, 2004]; (second row) wind speed-dependent piston velocity k_w used in the model (note this is very low in regions with extensive sea ice; regions of permanent sea ice not shown); (third row) the ratio of mixed layer depth to piston velocity, which would give the equilibration timescale of CO_2 in the mixed layer if it did not react with water (in days); (fourth row) the DIC/CO_2 ratio from the control simulation; (fifth row) the product of z_{ML}/k_w and DIC/CO_2 which gives the local equilibration timescale of carbon isotopes $\tau_{\delta DIC}$ (in days). See also *Jones et al.* [2014] for a similar calculation.

the entire ocean depleted, with greater depletion in waters that are more isolated from the atmosphere. Because the surface ocean disequilibria for both isotopes are large, the pCO_2 effect can play a first-order role in the global distribution of carbon isotopes, by modifying the intensity of the disequilibria.

Below, we first elaborate on the theoretical basis for why a higher pCO_2 causes the carbon isotopic ratios of seawater to equilibrate more quickly with the overlying atmosphere. We then use numerical modeling to estimate the ensuing repartitioning of carbon isotopes between the surface ocean, deep ocean, and atmosphere. The numerical results show relatively predictable changes in the distribution of $\delta^{13}C$ and $\Delta^{14}C$, in good agreement with the theory, that should be considered when interpreting isotopic records from any periods of Earth history during which pCO_2 differed significantly from the preindustrial.

2. Theory

In the absence of other sources or sinks and ignoring mixing with underlying waters, the time evolution of the surface mixed layer concentration of a gas (defined as C) due to exchange with the atmosphere can be approximated by the following time-dependent equation:

$$\frac{\partial C_{ocean}}{\partial t} = \frac{k_w}{z_{ML}}(C_{sat} - C_{ocean}) \qquad (1)$$

where k_w is the gas exchange coefficient (also known as the piston velocity, in m s^{-1}), largely dependent on the wind speed at the sea surface [*Wanninkhof*, 1992], and z_{ML} is the thickness of the mixed layer at the surface of the ocean (in meters) [*Sarmiento and Gruber*, 2006]. $(k_w/z_{ML})^{-1}$ is therefore the *e*-folding equilibration timescale with which the mixed layer concentration C_{ocean} will approach the saturation concentration that would be in equilibrium with the atmosphere, C_{sat} (Figure 1).

However, unlike most gases, CO_2 reacts with water as it dissolves. The reaction product, H_2CO_3, then dissociates to form HCO_3^- and CO_3^{2-}. At seawater pH, the total dissolved carbon pool is dominated by HCO_3^- and CO_3^{2-}, yet all of the air-sea exchange must pass through the bottleneck of CO_2. As detailed in the appendix, this unusual feature causes the equilibration *e*-folding timescale of DIC between seawater and air in the mixed layer (τ_{DIC}) to scale as

$$\tau_{DIC} = \left(\frac{\partial DIC}{\partial CO_{2ocean}}\right) \cdot \left(\frac{k_w}{z_{ML}}\right)^{-1} \qquad (2)$$

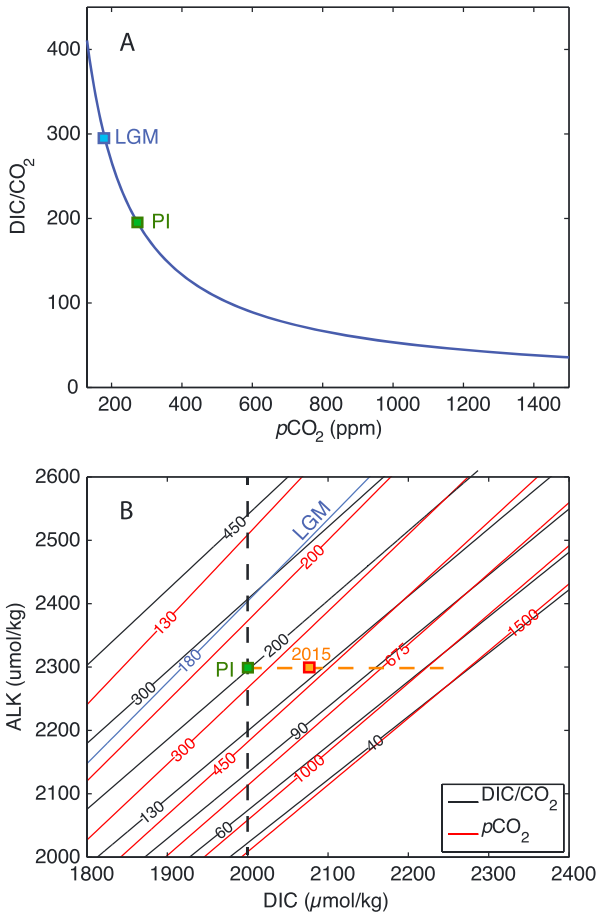

Figure 2. Variations of DIC/CO_2 in seawater at equilibrium. (a) How DIC/CO_2 varies with atmospheric pCO_2 for a constant DIC concentration of 2000 μM. (b) How DIC/CO_2 and pCO_2 vary with alkalinity (ALK) and DIC concentrations at equilibrium with a uniform ocean surface. Black contours show DIC/CO_2; red contours show pCO_2. The green squares in Figures 2a and 2b approximately correspond to the low-latitude ocean in the preindustrial state, while the blue squares in Figure 2a and blue line in Figure 2b approximately correspond to the LGM low-latitude surface ocean. The dashed vertical line in Figure 2b corresponds to the DIC/CO_2 versus pCO_2 section shown in Figure 2a. The horizontal orange line in Figure 2b corresponds to the current anthropogenic fossil fuel release, ignoring carbonate compensation, while the orange square corresponds to the low-latitude ocean in 2015.

where CO_{2ocean} is the concentration of dissolved CO_2 gas in the mixed layer. Because the buffer capacity ($\partial DIC/\partial CO_{2ocean}$) is ≈ 20 in the modern ocean, the equilibration timescale of CO_2 is typically ≈ twentyfold slower than nonreactive gases such as oxygen [*Broecker and Peng*, 1974; *Sarmiento and Gruber*, 2006].

The same chemical bottleneck that applies to the abundant stable isotope ^{12}C also applies to the less abundant ^{13}C and the radioisotope ^{14}C. However, the relative abundances of ^{13}C and radiocarbon (^{14}C) are expressed as ratios with ^{12}C ($\delta^{13}C$ and $\Delta^{14}C$, respectively), and, somewhat nonintuitively, the isotopic ratios follow a distinct equilibration timescale. As shown in the appendix, this equilibration timescale can be approximated by

$$\tau_{\delta DIC} = \frac{DIC}{CO_{2ocean}} \cdot \left(\frac{k_w}{z_{ML}}\right)^{-1} \quad (3)$$

Thus, rather than depending on the buffer capacity, the equilibration timescale of the carbon isotopic ratios in the mixed layer scales linearly with the ratio of DIC to dissolved CO_2. In the modern ocean this ratio is, on average, ≈ 200 (Figure 1) such that the timescale turns out to be about tenfold slower than the equilibration timescale for CO_2 [*Broecker and Peng*, 1974; *Jones et al.*, 2014].

The ratio DIC/CO_2 is determined by the concentrations of DIC and alkalinity, with a secondary effect from temperature and salinity. Because the proportion of DIC present in the form of dissolved CO_2 is so small, it has a lot of leeway to adjust to changes in speciation so that CO_2 can change many fold with very little change in DIC. Figure 2a illustrates this point, showing the DIC/CO_2 ratio expected for seawater at equilibrium with a range of atmospheric pCO_2, achieved by varying alkalinity given a typical modern DIC concentration of 2000 μM and constant temperature and salinity. Since oceanic DIC concentrations may also have changed significantly over time and are increasing now due to human activities, it is useful to consider how varying the global DIC inventory might alter the dissolved DIC/CO_2 relationship with atmospheric pCO_2. Figure 2b shows a range of solutions for seawater DIC/CO_2 for a matrix of simultaneous changes in DIC and alkalinity. As shown by the red and blue lines, changes in pCO_2 and DIC/CO_2 ratio are nearly parallel over a range of DIC and alkalinity. Given the nearly parallel slopes, the isotopic equilibration timescale can be predicted relatively well by the pCO_2 alone, with a small deviation to relatively slower equilibration under higher alkalinity and DIC for a given pCO_2.

The changes in isotopic equilibration timescale implied by Figure 2 are quite large. For example, under the pCO_2 of the Last Glacial Maximum (LGM), with no change in k_w/z_{ML}, the simple theory predicts that the

isotopic equilibration timescale would have been approximately 50% longer than the preindustrial case, while under a pCO_2 of 1500 ppm, which may have occurred during intervals of the early Cenozoic, the isotopic equilibration timescale would have been only one fifth that of the preindustrial. We emphasize that these changes arise purely as a result of shifts in the speciation of DIC under different pCO_2 and would occur independently of any changes in ocean circulation, wind speeds, or the biological pump. The final result of these changes in gas exchange timescale on the distribution of carbon isotope ratios is different for the two carbon isotope systems and depends on global mass balance and the effect of ocean circulation, creating a nontrivial problem. We address the problem with numerical models.

3. Models

The pCO_2 effect is simulated by any model that fully resolves the carbonate equilibria and air-sea exchange. As such, in any simulation that causes a significant surface CO_2 change, the disequilibrium should respond, even though the authors of the simulation may not have explicitly identified the contribution of the speciation to the overall result [e.g., *Huiskamp and Meissner*, 2012; *Kohler et al.*, 2006]. In contrast, simplified analog tracers, which do not resolve the carbonate equilibria, would miss the speciation effect entirely [e.g., *Schmittner*, 2003]. In addition, experiments that change only atmospheric $\Delta^{14}C$ to, for example, glacial values without making a corresponding change in pCO_2 would have missed this effect [e.g., *Franke et al.*, 2008].

Here an equilibrium solution to a three-dimensional general circulation model is used to gain a better understanding of the pCO_2 effect. The model uses an off-line transport model [*Primeau*, 2005] coupled with a simple ocean biogeochemistry model from the second phase of the Ocean Carbon Model Intercomparison Project (OCMIP2) [*Najjar et al.*, 2007]. The horizontal resolution is 3.75°, and the vertical resolution decreases from 50 m near the surface to 300 m near the bottom. The biogeochemical model parameters have been optimized with respect to observed climatological data of phosphate, alkalinity, and DIC [*Kwon and Primeau*, 2008]. The model solves for an equilibrium using a time-efficient solver [*Kwon and Primeau*, 2008]. The rapid calculation of the equilibrium allows for multiple sensitivity runs to be conducted within only a few days, which makes it ideally suited for this study. Tracers for the dissolved inorganic carbon isotopes ($DI^{13}C$ and $DI^{14}C$) have been added. The small mass-dependent kinetic and equilibrium fractionations of ^{14}C that occur during air-sea exchange and biological cycling are ignored, since these are (at least partly) removed by the $\delta^{13}C$ correction applied in the reporting convention of $\Delta^{14}C$ [*Stuiver and Polach*, 1977]. The model simulates ^{13}C following *Schmittner et al.* [2013]. A temperature-dependent equilibrium fractionation occurs during air-sea gas exchange, using the experimentally determined fractionation factors of *Zhang et al.* [1995]. The photosynthetic fractionation factor ϵ_p is parameterized following *Popp et al.* [1989], which depends on the CO_{2ocean} concentration in each grid cell.

The pCO_2 effect should be expressed under any change in the global carbon cycle that alters atmospheric pCO_2. However, some degree of complication could be expected given that the equilibration timescale depends on CO_{2ocean}/DIC, and concentrations of DIC as well as the CO_2 disequilibrium at the ocean surface could change. In order to test this, idealized experiments were conducted with the model that modify the preindustrial carbon cycle in three different ways. First, the globally averaged alkalinity concentration was varied between −420 and +270 μM relative to preindustrial in increments of 30 μM (experiment *alk*). Second, the globally averaged $DI^{12}C$ and $DI^{13}C$ concentrations were varied simultaneously by between −210 and +420 μM relative to preindustrial in increments of 30 μM, while maintaining a constant global ratio of $^{13}C/^{12}C$ and a constant ^{14}C inventory (experiment *dic*). Third, the biological storage of carbon in the ocean was changed by altering the surface PO_4 concentrations to which simulated PO_4 is restored, by a factor of 0 to 1.6, in increments of 0.1 (experiment *pref*); a factor of 0 corresponds to a maximum of export production from the surface, decreasing as the multiplier increases. These ranges were chosen to exceed the glacial-interglacial change, while the dic and alk experiments span the early Cenozoic and near-future changes of pCO_2 as well. Although the mechanisms are all potentially relevant to the glacial-interglacial change and to the more distant geological past, as well as the future, the experiments are not intended to accurately simulate any particular state of the carbon cycle but rather to test the consistency of the theorized pCO_2 effect under a range of altered carbon cycle states. We also included experiments in which we changed the carbon speciation directly by modifying the pH used in the speciation calculation used to determine CO_{2ocean} during air-sea exchange, over a range of −1.1 to +0.5 relative to preindustrial (experiment *pH*). Thus, no matter what the surface ocean DIC might be, the surface ocean pH is set equal

to that of the same surface grid cell in the control simulation plus the imposed change in pH. The pH experiment thereby manipulates the DIC/CO_2 independent of changes in the DIC and alkalinity concentrations in order to evaluate the effect of the "pure" pCO_2 effect. In order to easily interpret the results of all experiments, the characteristics of the "low-latitude surface" layer are averaged over the latitudinal range 40°S to 40°N, and the "deep ocean" is averaged globally below 1000 m depth.

The steady state model can efficiently compute the equilibrium state, but it cannot evaluate the transient response of radiocarbon to environmental changes. In addition, one might worry that a host of unresolved processes might confound the expression of the speciation effect on radiocarbon distributions in the real world, particularly under changing environmental conditions. In particular, changes in cosmogenic ^{14}C production, changes in ocean circulation, and the production and dissolution of $CaCO_3$ sediment could all complicate the picture. We illustrate the transient response of radiocarbon to rapid pCO_2 changes, as well as the combined result of multiple factors over the deglaciation, using the CYCLOPS 18-box ocean model (described by *Hain et al.* [2010]). CYCLOPS includes sediment interactions (the sedimentation and dissolution of $CaCO_3$ at the seafloor) and variations in radiocarbon production and can be run in a transient mode over tens of thousands of years. The results shown in Figure 9 are from the previously published "North Atlantic circulation change + Southern Ocean CO_2 release" deglacial scenario from *Hain et al.* [2014].

The remainder of this paper discusses how the numerical model simulations alter the distribution of $\delta^{13}C$ and $\Delta^{14}C$ between the ocean and atmosphere. Because the mechanisms of disequilibrium for $\delta^{13}C$ and $\Delta^{14}C$ are so different, we treat each isotope ratio in turn.

4. The pCO_2 Effect and Radiocarbon

Radiocarbon is produced in the upper atmosphere from cosmic rays. But because of the high solubility of CO_2 in seawater, most of the ^{14}C in the Earth system is dissolved in the ocean. It decays with a half-life of 5730 years, leading to the loss of ^{14}C from throughout the ocean interior, which is balanced by a downward flux of ^{14}C across the air-sea interface. Because the air-sea equilibration timescale is slow, the surface ocean ^{14}C concentration remains well below equilibrium with respect to the atmosphere. The estimate of *Key et al.* [2004] suggests that, prior to aboveground nuclear testing, the globally averaged $\Delta^{14}C$ of the surface ocean was about −65‰ (i.e., 6.5% depleted relative to the nineteenth century atmosphere), equivalent to the decay loss that would occur over ≈550 years. Over the time span for which radiocarbon is a useful tool (the past ≈50 kyr [*Reimer et al.*, 2013]), pCO_2 has undergone significant changes. The fact that surface ocean DIC/CO_2 must have changed along with the atmospheric pCO_2 has clear implications for the air-sea partitioning of radiocarbon, and for the use of radiocarbon as a chronometer and monitor of ocean circulation in marine archives.

4.1. Air-Sea Redistribution

Under lower pCO_2, high DIC/CO_2 will slow the equilibration of radiocarbon in the mixed layer, according to the theory (Figure 2a). This leaves more ^{14}C behind in the atmosphere, driving up atmospheric $\Delta^{14}C$. At steady state, the total decay of ^{14}C in the ocean, equal to the product of the decay rate constant λ, and the oceanic ^{14}C inventory (M_{14C}) must be balanced by the net flux of ^{14}C into the ocean (F_{14C}), integrated globally:

$$\int F_{14C} = \lambda M_{14C} \tag{4}$$

Given the reduced exchange rate that accompanies a lower pCO_2, the required $\int F_{14C}$ must be accomplished by raising the atmospheric concentration of $^{14}CO_2$, and thus, raising $^{14}CO_{2sat}$, until the intensified air-sea concentration gradient ($^{14}CO_{2sat} - {}^{14}CO_{2ocean}$) compensates for the reduced exchange rate.

This simple dynamic is clearly expressed in the results of the model simulations, shown in Figure 3. As expected, a decrease of pCO_2 impedes the oceanic uptake of atmospheric ^{14}C, raising atmospheric $\Delta^{14}C$, while the fact that most of the total carbon inventory is in the ocean prevents the $\Delta^{14}C$ of the ocean from changing significantly. The good agreement between the pref, alk, and pH experiments supports the general robustness of the theory regardless of the mechanism behind the pCO_2 change, and because the pH experiment changes only the carbon speciation in surface waters, it shows explicitly that the pCO_2

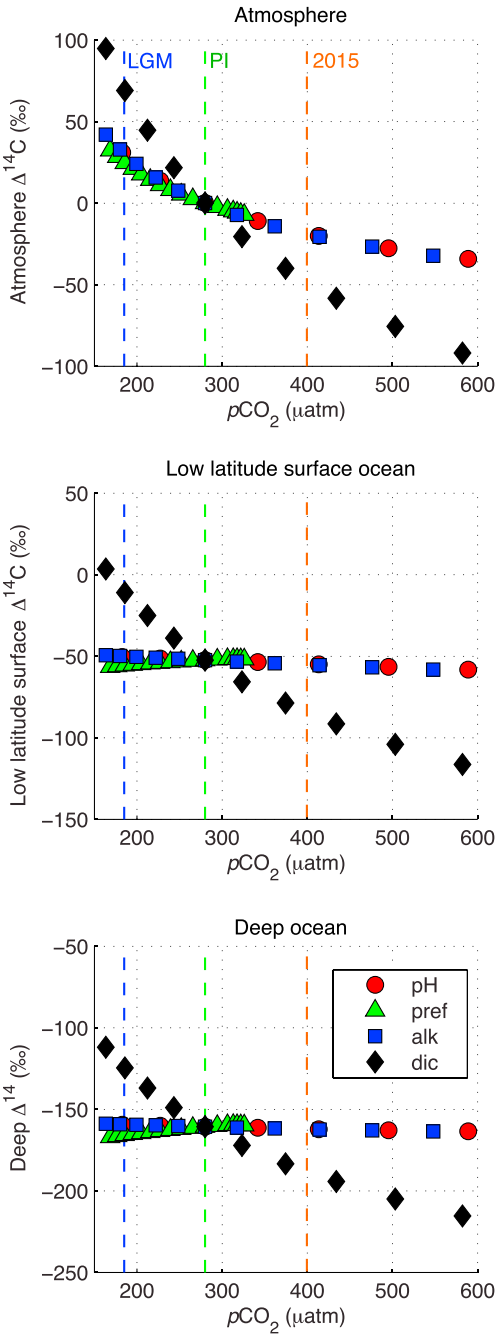

Figure 3. The effect of the simple experiments on $\Delta^{14}C$ versus pCO_2 in the model. (top) The atmospheric $\Delta^{14}C$, (middle) the low-latitude surface ocean $\Delta^{14}C$, and (bottom) the deep ocean $\Delta^{14}C$. The experiments modify the carbon cycle in four different ways, as described in the methods, to achieve a range of changes in air-sea partitioning. The dic experiments follow a distinct trend because they involve variable dilution of the constant global ^{14}C inventory with ^{12}C, whereas global $^{14}C/^{12}C$ is constant in the other experiments. The dashed vertical lines indicate the pCO_2 of the Last Glacial Maximum (blue) and preindustrial (green).

effect is the driver of the changes. The exception to the general picture is the dic experiment, in which the total carbon inventory was varied, since a larger carbon inventory dilutes the constant global inventory of radiocarbon, lowering $\Delta^{14}C$ throughout the ocean and atmosphere as the DIC inventory grows.

When the oceanic values are expressed as the difference from the corresponding atmospheric $\Delta^{14}C$ ($\Delta\Delta^{14}C$) in Figure 4, an even simpler picture emerges. In this case, the oceanic values of experiment dic fall in line with the other experiments, since the dilution effect is equally applied to the ocean and atmosphere. Note that Figure 4 is now plotted versus the inverse of pCO_2; since the surface DIC varies by only a few percent among these experiments, the relatively large changes in pCO_2 drive the changes in DIC/CO_2, so that the relationship between the disequilibrium and $1/pCO_2$ is approximately linear. Additional experiments show that the effect is roughly proportional to the total ^{14}C inventory: if the inventory is increased by 23 %, as it may have during the LGM [*Hain et al.*, 2014], the magnitude of the pCO_2 effect increases by a similar amount, as indicated by the red symbols in Figure 4.

One outstanding problem in the understanding of radiocarbon is the high $\Delta^{14}C$ of the LGM atmosphere, which was more than 400‰ higher than the preindustrial atmosphere [*Ramsey et al.*, 2012; *Southon et al.*, 2012]. High production rates of ^{14}C during the glacial period certainly contributed to the high $\Delta^{14}C$ and were most likely the main cause [*Hain et al.*, 2014]. However, reconstructions of the production rate, derived from ^{10}Be measured in Greenland ice cores [*Muscheler et al.*, 2004] and geomagnetic field reconstructions [*Laj et al.*, 2004], appear to explain no more than 300‰ of the increase, leaving a >100‰ gap [*Broecker and Barker*, 2007; *Skinner et al.*, 2010; *Hain et al.*, 2014]. Although debatable, sluggish ventilation of the deep ocean during the glacial probably played a large role in closing the gap, by transporting less ^{14}C into the deep sea [*Galbraith et al.*, 2007; *Broecker et al.*, 2008; *Lund et al.*, 2011; *Burke and Robinson*, 2012; *Hain et al.*, 2014]. The dashed vertical blue line in Figure 3 indicates the $1/pCO_2$ that corresponds to the LGM and shows that according to the model the pCO_2

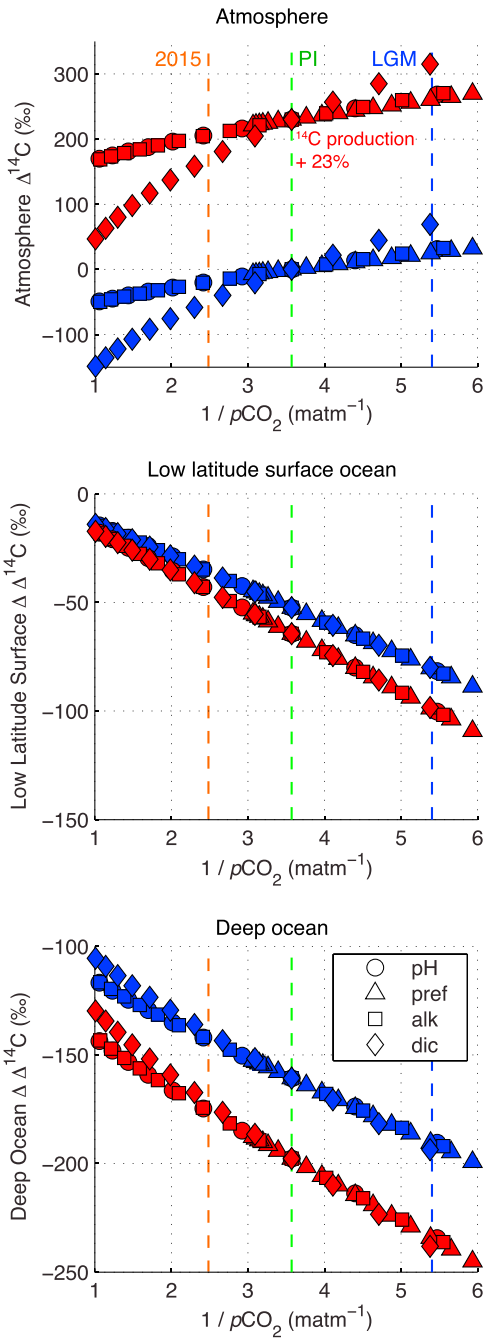

Figure 4. Changes in the air-sea disequilibrium in the model, and impact of production rate. The blue symbols show the same results as in Figure 3, now plotted versus $1/pCO_2$ on the abscissa, and with the oceanic values referenced to the corresponding atmospheric $\Delta^{14}C$ (referred to as the $\Delta\Delta^{14}C$). In addition, the plots include an identical suite of experiments in which the production rate of ^{14}C was increased by 23% (red symbols), as possibly occurred during the LGM. The dashed vertical lines indicate the $1/pCO_2$ of the LGM (blue) and preindustrial (PI) (green).

effect would have raised the atmospheric $\Delta^{14}C$ by ≈ 30‰ relative to the preindustrial (the dashed vertical green line). If combined with a 23% increase of ^{14}C production, the pCO_2 effect is amplified proportionally, resulting in an increase of ≈ 37‰. Thus, although of secondary importance, the pCO_2 effect would have contributed to closing the gap during the LGM.

The model also predicts the spatial patterns of the pCO_2 effect on oceanic $\Delta^{14}C$, under the assumption of constant ocean circulation. Figure 5 shows the change in $\Delta\Delta^{14}C$ (relative to the atmosphere) for the pure pCO_2 effect, in which the pH used to calculate the carbonate equilibria was increased in all surface grid cells by 0.20, approximately corresponding to the LGM pCO_2 in this model (183 µatm). Because the pCO_2 effect primarily acts by shifting the overall air-sea balance of radiocarbon, it has little impact on the spatial gradients of radiocarbon within the ocean (<7‰), compared to the corresponding increase in atmospheric $\Delta^{14}C$ (>30‰). The changes that do occur are dominated by the fact that the relatively well-equilibrated North Atlantic responds less to the pCO_2 effect than does the poorly equilibrated Southern Ocean. Thus, the air-sea redistribution of radiocarbon that follows from the low pCO_2 of the LGM would have caused atmospheric $\Delta^{14}C$ to rise with a negligible increase of the age differences between coeval benthic and planktonic foraminifera. As such, its contribution to the deglacial changes in atmospheric $\Delta^{14}C$ would not have incurred any change in the benthic-planktonic age differences, helping to reconcile the equivocal glacial-interglacial contrasts in benthic-planktonic ages that appear to typify many parts of the ocean [*Broecker et al.*, 2008]. This also means the pCO_2 effect would not have contributed significantly to the high glacial $\Delta^{14}C$ recorded in biogenic carbonates of the open ocean surface, such as planktonic foraminifera or corals [e.g., *Hughen et al.*, 2004]. Rather, its contribution applies to radiocarbon measured in archives that formed from waters with small reservoir ages [e.g., *Ramsey et al.*, 2012; *Southon et al.*, 2012].

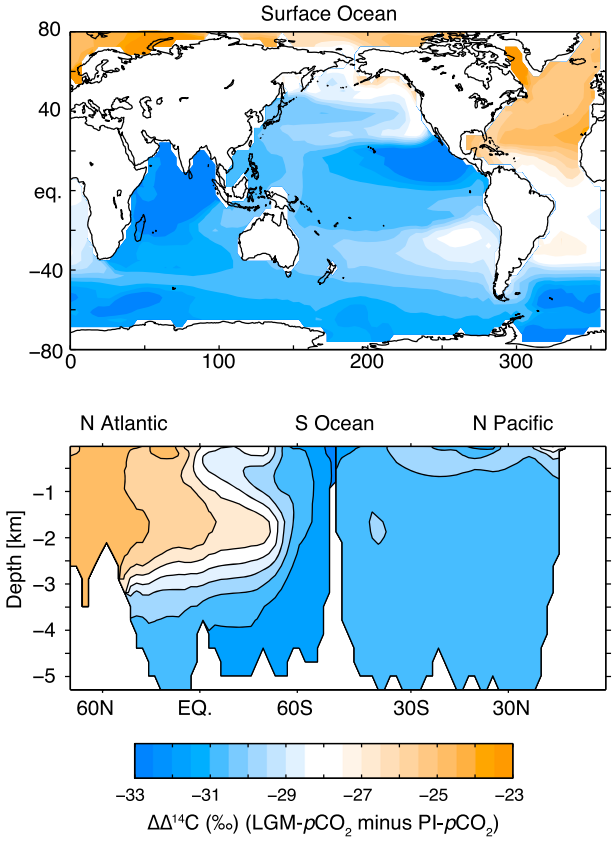

Figure 5. Spatial variability of changes in $\Delta\Delta^{14}C$ under LGM pH in the model. The two panels show the difference of $\Delta\Delta^{14}C$ between the LGM-pCO_2 experiment and the control (in ‰), for the (top) surface ocean and for a (bottom) zonal average of the Pacific and Atlantic Ocean basins. The oceanic $\Delta\Delta^{14}C$ is lower everywhere due to enhanced disequilibrium caused by low pCO_2, an effect that is more pronounced in the strongly unequilibrated waters of the Southern Ocean.

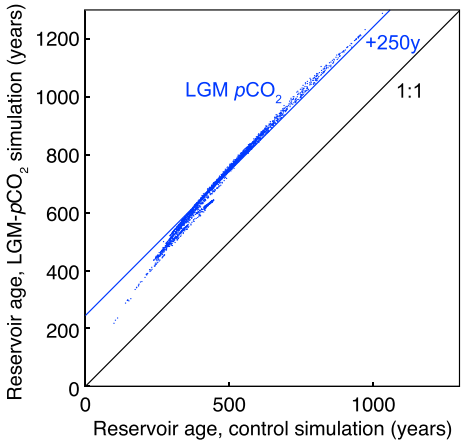

Figure 6. Surface reservoir ages under LGM pCO_2 in the model. Each blue dot corresponds to one location on the ocean surface, with the reservoir age from the preindustrial control simulation shown on the *x* axis, and the corresponding LGM reservoir age shown on the *y* axis. The LGM points lie approximately 250 years above the 1:1 line.

4.2. Effect on Surface Reservoir Age

The pCO_2 effect has implications for the calculation of chronological ages using surface ocean $\Delta^{14}C$ measurements in fossil carbonate. Any such calculation requires a correction for the local reservoir age, i.e., the apparent age of DIC in surface waters during calcification, a function of the disequilibrium relative to the contemporaneous atmospheric $\Delta^{14}C$. In the modern ocean, this is typically assumed to be on the order of 400 years throughout most of the low latitudes [*Reimer et al.*, 2004], and it is often assumed that this would have remained constant over time, in the absence of further information. Given the pCO_2 of the LGM, if the ocean circulation were unchanged from today, and the system were at steady state, the model simulation suggests that global reservoir ages would have increased by approximately 250 years due to the pCO_2 effect alone (Figure 6). Because of the uniform nature of the $\Delta^{14}C$ change (shown in Figure 5), the increase of reservoir age is also uniform. In agreement with this estimate, the reconstructed LGM-Holocene difference in surface reservoir ages of the Cariaco Basin, Barbados, and the tropical Pacific are all consistent with a change of 250 years [*Ramsey et al.*, 2012]. As atmospheric pCO_2 rose during the deglaciation, the pCO_2 effect's contribution to the surface reservoir age would be expected to have decreased in concert, as a linear function of $1/pCO_2$.

It is important to emphasize that this change in surface reservoir age is not a firm prediction, given that ocean circulation is sure to have varied to some degree: regions with surface mixed layers that entrained much less ^{14}C-depleted deep water, relative to today, could have been better equilibrated with the atmosphere. Conversely, greater depletion may have occurred in regions that were in stronger communication with

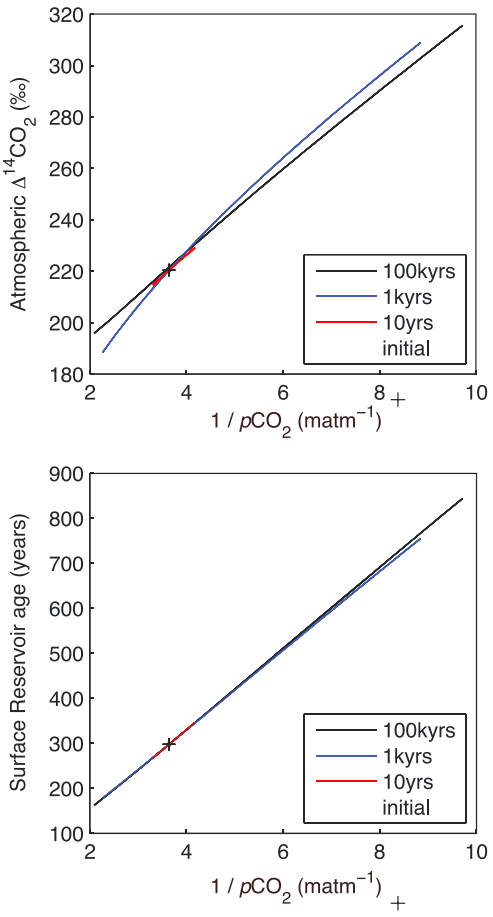

Figure 7. The transient response of the CYCLOPS model to surface ocean speciation. Each colored line shows the response after a given number of years to a spectrum of instantaneous changes of pH, imposed abruptly on a preindustrial state. The pH changes directly manipulate the carbon speciation, altering atmospheric pCO_2 and the air-sea partitioning of radiocarbon. As shown by the suite of simulations, the response of the (top) atmospheric $\Delta^{14}C$ and (bottom) surface reservoir age occurs just as rapidly as the change in pCO_2 so that the 10 year response is nearly indistinguishable from the steady state response.

^{14}C-depleted deep waters, particularly if those deep waters were very strongly depleted, or where sea ice was more extensive, as has been suggested for the LGM Southern Ocean [*Skinner et al.*, 2010]. The globally uniform pCO_2-based estimate here should be taken as an expected baseline, for which circulation did not change, and under steady state.

4.3. Robustness of the Speciation Effect During Transient Changes

Thus far, the pCO_2 effect has been discussed as a steady state phenomenon. However, radiocarbon requires many thousands of years to fully equilibrate throughout the Earth System, including the slow adjustment of the deep ocean reservoir and interaction with carbonate sediments, raising the question of to what degree the pCO_2 effect would have been expressed during real geological transients. We address this question using the CYCLOPS model.

The first set of experiments changes the speciation of carbon in the surface ocean instantaneously by overriding the pH used in the carbon system calculations, similar to the pH experiments of the three-dimensional model discussed above. Following the pH change, CYCLOPS is run to equilibrium. The results in Figure 7 show the atmospheric $\Delta^{14}C$ and surface ocean reservoir ages versus $1/pCO_2$ after 10, 1000, and 100,000 years. Perhaps surprisingly, the results all fall very close to the same relationship as the equilibrium state: after 10 years the surface ocean and atmosphere appear to be quite well equilibrated. How can this be?

The answer lies in the fact that it is the atmospheric radiocarbon pool that changes in response to the surface ocean carbon speciation. In these experiments, the constant ^{14}C production rate requires the amount of radiocarbon in the ocean to remain roughly constant at equilibrium, since the decay of global ^{14}C must balance atmospheric production and almost all of the ^{14}C is in the ocean. As a result, the relative change in the ^{14}C content of the ocean is very small. In contrast, given the small mass of atmospheric carbon—and the fact that it is all CO_2 in the atmosphere, no carbonate chemistry required—the atmospheric ^{14}C can be changed significantly and virtually instantaneously [*Hain et al.*, 2011]. So when the surface ocean speciation causes the atmospheric pCO_2 to drop, slowing the uptake of ^{14}C by the ocean, ^{14}C builds up in the atmosphere very quickly, approaching steady state within a few years. This implies that the pCO_2-induced reservoir age changes discussed in section 4.2 are robust even in the face of transient CO_2 changes.

A second type of experiment introduces the additional complexities of changes in ^{14}C production, ocean circulation, and interaction with sediments, using one of the postulated deglacial transitions of *Hain et al.* [2014]. The deglacial scenario arbitrarily imposes a breakdown of stratification, a decrease of nutrient consumption, and a retreat of sea ice in the Southern Ocean, all of which release CO_2 to the atmosphere, as well

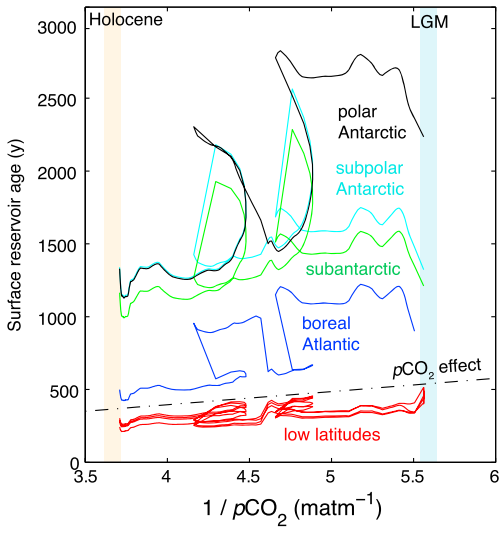

Figure 8. Simulations of surface reservoir ages in the CYCLOPS model throughout a deglacial scenario. Each line traces the complete deglacial transient in one surface box, as labeled, starting at the high LGM $1/pCO_2$ and progressing to the low Holocene $1/pCO_2$. Sharp changes in the polar boxes are caused by imposed circulation changes, while additional wiggles are produced by variations in ^{14}C production rates and changes in carbonate sedimentation. Despite these complexities, the overall trend of the low-latitude surface boxes agrees well with the slope expected from the steady state relationship, shown by the dash-dotted black line.

as drastic changes in circulation that represent stalling and reinvigoration of the Atlantic Meridional Overturning Circulation. The scenario also imposes data-constrained fluctuations in ^{14}C production, which help to simulate the observed decrease of atmospheric $\Delta^{14}C$ of 350‰ over the deglaciation, as detailed by *Hain et al.* [2014].

Figure 8 shows the resulting reservoir ages from this simulation, where each continuous line traces the evolution of one surface box over the deglacial transient, plotted versus the corresponding $1/pCO_2$. The imposed changes in the circulation geometry of North Atlantic waters introduce dramatic swings in the reservoir ages of the polar ocean surface boxes, reflecting the importance of mixing between surface boxes and the ^{14}C-depleted deep ocean. Meanwhile, the low-latitude surface follows the trend of the expected (dash-dotted) curve faithfully. Importantly, the modeled low-latitude reservoir ages fall ≈ 100 years below the steady state trend, largely attributable to the decreasing atmospheric ^{14}C production throughout the simulation; because the oceanic inventory remembers the atmospheric $\Delta^{14}C$ of prior millennia, it is biased high when atmospheric $\Delta^{14}C$ is on a decreasing trend, equating to a relatively low reservoir age [*Franke et al.*, 2008]. Thus, this experiment supports the utility of the pCO_2-based reservoir age prediction for sites at which circulation changes were small, while also illustrating the importance of transient changes in ^{14}C production [*Beer et al.*, 1988; *Franke et al.*, 2008], and the potential for dramatic excursions from the pCO_2-based baseline wherever the exposure of deep, ^{14}C-depleted waters changes over time [*Skinner et al.*, 2010; *Sarnthein et al.*, 2007].

4.4. Effect on the Modern and Future Ocean

Finally, we show how the anthropogenic pCO_2 rise has accelerated the air-sea equilibration of radiocarbon relative to the preindustrial ocean, an acceleration that will continue in the future as long as pCO_2 continues to rise. Although, for the time being, this effect remains swamped by the aftermath of the bomb ^{14}C peak, it will become increasingly evident as the bomb carbon is dissipated within the oceans and as surface DIC/CO_2 continues to drop.

As illustrated by the pH experiments in Figure 3, the pCO_2 effect would be expected to lower the atmospheric $\Delta^{14}C$ by ≈ 20‰, relative to the preindustrial state, given the year 2015 atmospheric pCO_2 of 400 μatm. Such a change is smaller than the Suess effect (i.e., the dilution of radiocarbon by the anthropogenic addition of ^{14}C-free fossil carbon [*Tans et al.*, 1979]), which would be expected to lower the surface ocean $\Delta^{14}C$ by an additional ≈ 30‰ at steady state, as illustrated by the DIC experiments in Figure 2. In reality, the Suess effect in the atmosphere is greatly amplified relative to the steady state solution by the fact that fossil fuels are input directly to the small atmospheric reservoir. By contrast, the pCO_2 effect will continue to grow as pCO_2 rises further and will become increasingly important as the fossil carbon is taken up by the ocean.

We note that because the uptake of bomb radiocarbon occurred under a pCO_2 that was already elevated relative to the preindustrial, it was taken up more quickly than the same mass of radiocarbon would have been taken up under preindustrial pCO_2 [*Siegenthaler*, 1986]. As a result, the pCO_2 effect must be included in any use of bomb radiocarbon together with natural ^{14}C measurements to calculate global air-sea exchange.

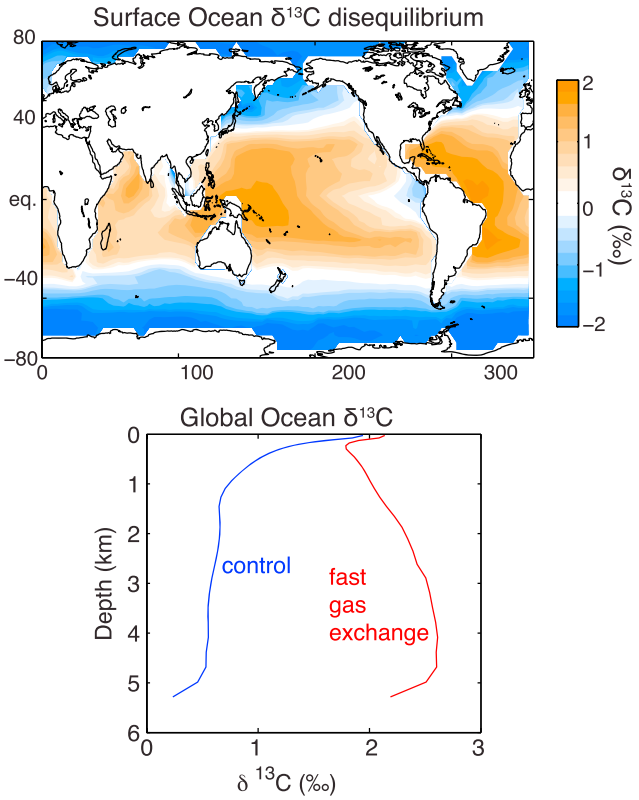

Figure 9. Disequilibrium of carbon isotopes in the ocean. (top) The surface ocean disequilibrium $\delta^{13}C$, estimated by subtracting a fast gas exchange simulation, in which the piston velocity was multiplied by 1000 and the atmospheric $\delta^{13}C$ held constant, from the control simulation. The carbon isotopic disequilibrium is negative at high latitudes and in low-latitude upwellings, and positive everywhere else. (bottom) Globally averaged vertical profiles of $\delta^{13}C$ in the control simulation and the fast gas exchange simulation. The vertical gradient is greatly reduced, or even reversed, with fast gas exchange, showing that the low $\delta^{13}C$ of the deep ocean is maintained by air-sea disequilibrium.

The effect should be implicit in pCO_2-dependent gross flux calculations [e.g., *Naegler et al.*, 2006], as well as OCMIP2-style calculations that include transient pCO_2 changes [e.g., *Müller et al.*, 2008].

5. The Speciation Effect and $\delta^{13}C$

We now turn to the case of the stable isotope ratio, $\delta^{13}C$. The surface disequilibrium of $\delta^{13}C$ is fundamentally different than that of radiocarbon, in that it exists as a spectrum from positive to negative values, as determined by the interplay between biological fractionation, temperature and salinity gradients, and ocean circulation [*Broecker and Maier-Reimer*, 1992; *Lynch-Stieglitz et al.*, 1995].

At thermodynamic equilibrium, ^{13}C is preferentially partitioned into colder water relative to warm water, with equilibrium $\delta^{13}C$ decreasing by 0.1‰ C^{-1} warming [*Mook et al.*, 1974]. Thus, if the ocean were at thermodynamic equilibrium, $\delta^{13}C$ would increase from the warm surface to the cold depths. However, because the equilibration timescale of $\delta^{13}C$ is so slow, only at the warm low latitudes are surface waters well equilibrated. Cooling of poleward advected waters prior to sinking is generally much faster than the modern equilibration timescale so that the cold waters that fill the deep ocean retain a low-$\delta^{13}C$ thermal disequilibrium component, a memory of the low latitudes [*Murnane and Sarmiento*, 2000]. This effect is generally accentuated by the "invasion" effect of [*Lynch-Stieglitz et al.*, 1995], which causes the DIC taken up during rapid cooling of surface waters to be closer to atmospheric $\delta^{13}C$ and therefore lower than the equilibrium $\delta^{13}C$.

Superimposed on the physical disequilibrium is the carbon isotope fractionation caused by the biological pump. Sinking organic matter has very low $\delta^{13}C$ (on the order of −25‰[*Rau et al.*, 1989; *Young et al.*, 2013]) so that its production raises the surface ocean $\delta^{13}C$ and its remineralization drives the deep ocean $\delta^{13}C$ to lower values. Because of the long equilibration timescale, brief exposure along outcrops of dense water in the Southern Ocean do little to erase this signature, allowing a disequilibrium to also build up from the biological pump, which is generally of the same sign as the thermal disequilibrium. Essentially, air-sea disequilibrium causes an underexpression of the thermal fractionation, and an overexpression of the biological fractionation, both of which cause the $\delta^{13}C$ of the deep sea to be low relative to the surface.

Although it cannot be observed directly, the disequilibrium effect can be estimated by comparing the preindustrial control simulation of the model with a "fast gas exchange" version in which the piston velocity, k_w, was multiplied by 1000. As shown in Figure 9 (top), the high-latitude surface ocean ^{13}C is 1–2‰ lower than it would be at equilibrium, while the low-latitude surface ocean is up to 2‰ higher than it would be at equilibrium. Figure 9 (bottom) shows that in the absence of disequilibrium, the thermodynamic enrichment of ^{13}C in deep waters and the biological buildup of ^{13}C-depleted carbon would very nearly cancel each

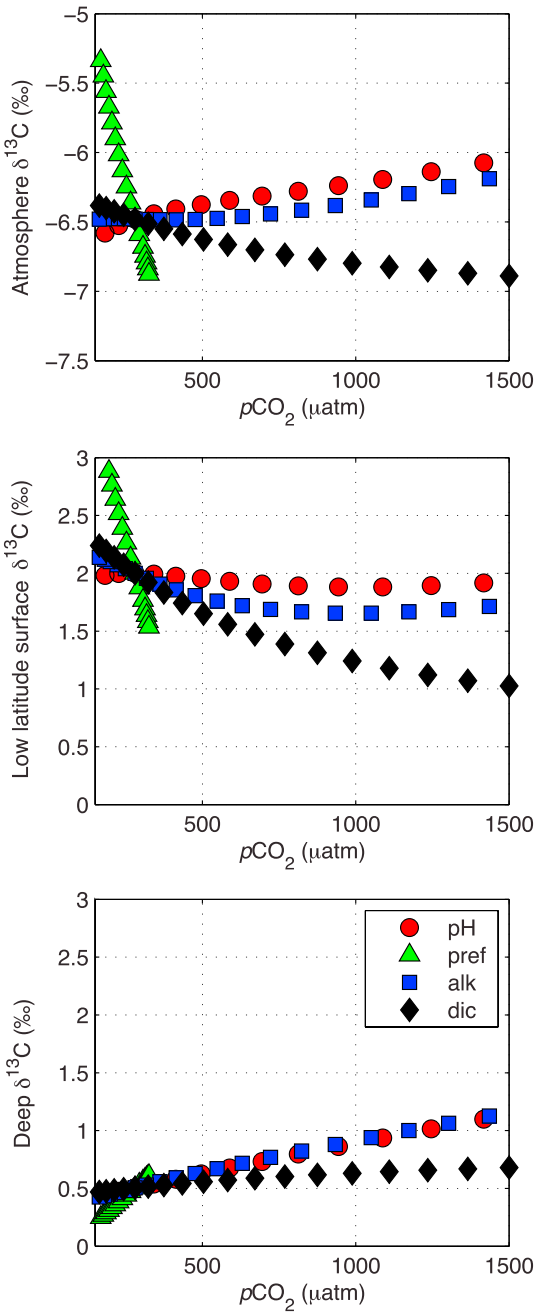

Figure 10. The effect of the simple experiments on $\delta^{13}C$ versus pCO_2 in the model. (top) The atmospheric $\delta^{13}C$, (middle) the low-latitude surface ocean $\delta^{13}C$, and (bottom) the deep ocean $\delta^{13}C$. Simulations here include variable ϵ_p.

other, resulting in a weak vertical $\delta^{13}C$ gradient. Although the importance of disequilibrium in setting the vertical profile will depend on the details of the numerical model to some degree, the results here agree qualitatively with the fast gas exchange experiments of *Schmittner et al.* [2013] and *Murnane et al.* [1999]. According to these models, it is essentially the long equilibration timescale of the carbon isotope ratios that causes $\delta^{13}C$ to decrease with depth in the modern ocean. The prominent role of disequilibrium in setting the vertical $\delta^{13}C$ gradient therefore introduces a large potential sensitivity to the pCO_2 effect.

Figure 10 shows the results for the idealized carbon cycle experiments with $\delta^{13}C$, analogous to Figure 3 for radiocarbon. In general, deep ocean $\delta^{13}C$ increases as pCO_2 increases, as the disequilibrium between high-latitude surface waters and the atmosphere is reduced, and as low-$\delta^{13}C$ carbon is transferred from the ocean to the atmosphere. In general, the results for $\delta^{13}C$ show more of a dependence on the particular mechanism of pCO_2 change than for radiocarbon, with a more significant spread between the experiments. In particular, for the pref experiments, for which pCO_2 is lowered by strengthening the biological pump, the direct pCO_2 effect or the air-sea equilibration timescale is overshadowed by the accelerated removal of low-$\delta^{13}C$ organic carbon from the upper ocean and sequestration at depth.

Again, to highlight the pCO_2 effect, we focus on the prescribed pH experiments. As shown in Figure 11, the redistribution has a clear global pattern. Under the low pCO_2 of the LGM, the pCO_2 effect decreases $\delta^{13}C$ in waters formed in the Southern Ocean relative to waters formed in the North Atlantic, enhancing the $\delta^{13}C$ contrast between these end-members by on the order of 0.2‰. This can explain approximately one fifth of the increased $\delta^{13}C$ gradient reconstructed from foraminifera in the glacial Atlantic [*Curry and Oppo*, 2005] with no change in the biological pump, ocean circulation, or sea ice. Going the other way, as pCO_2 becomes very high, the gradient between the surface and deep ocean becomes weak (Figure 12). The gradient is decreased by the gradual elimination of the disequilibrium component, allowing the thermodynamic fractionation to be more strongly expressed and reducing the overexpression of the biological pump.

It is important to consider that the expression of the pCO_2 effect depends on the response of the photosynthetic fractionation factor, ϵ_p, to pCO_2. Our model uses the *Popp et al.* [1989] relationship between ϵ_p and

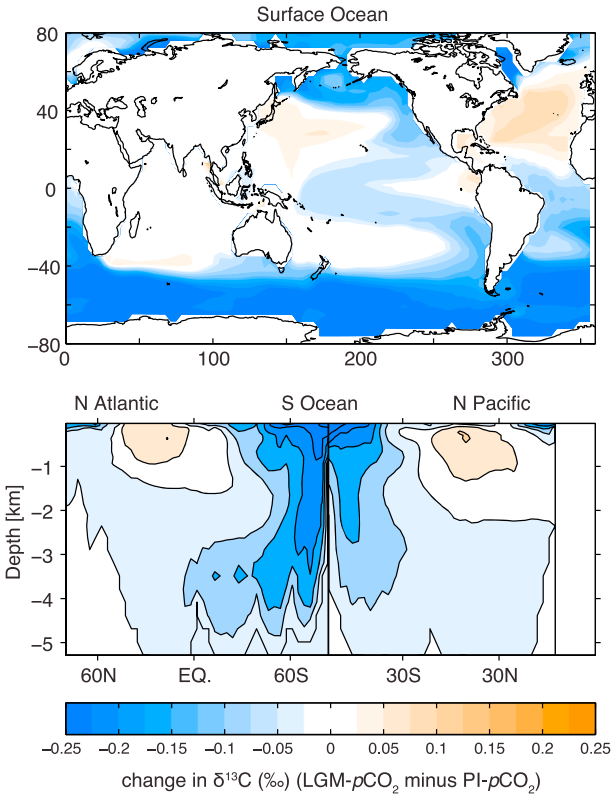

Figure 11. Spatial variability of changes in $\delta^{13}C$ under LGM pCO_2 in the model. Shading (in ‰) shows the variable ϵ_p simulation pH+0.2 relative to the preindustrial. (top) The surface ocean change; (bottom) change in zonal averages of the Atlantic and Pacific Ocean basins.

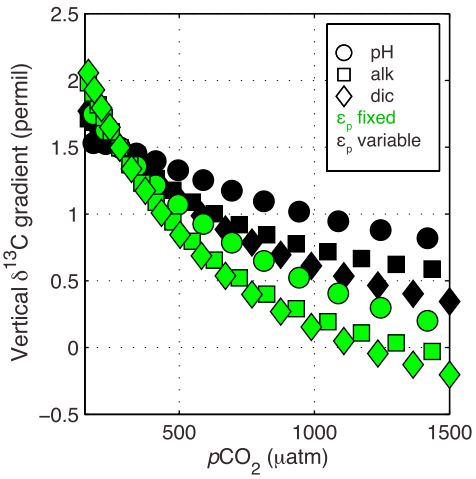

Figure 12. Modification of the vertical oceanic $\delta^{13}C$ gradient by pCO_2. Results from the model (Figure 9) are replotted here (black symbols) to emphasize the degree to which pCO_2 alters the vertical $\delta^{13}C$ gradient, in the absence of any change in the biological pump or ocean circulation. In addition, green symbols show identical simulations in which ϵ_p is held constant, thereby increasing the importance of the pCO_2 effect.

pCO_2, which predicts an increase of ϵ_p with increasing pCO_2, counteracting the pCO_2 effect on disequilibrium. However, this relationship has been questioned, based on laboratory experiments [e.g., *Burkhardt et al.*, 1999]. To illustrate the importance of this uncertain factor, Figure 12 shows the pCO_2 effect on the vertical $\delta^{13}C$ gradient that would occur with the variable *Popp et al.* [1989] relationship, as well as with ϵ_p fixed at the values used in the control simulation for all experiments. If ϵ_p does vary less than predicted by the *Popp et al.* [1989] relationship, the pCO_2 effect would be stronger than those shown in Figures 10 and 11.

The results here suggest that the pCO_2 effect had a small, but significant imprint on foraminiferal $\delta^{13}C$ records from the last glacial period. However, the large effect of pCO_2 on $\delta^{13}C$ distributions could be much more important for the interpretation of foraminiferal $\delta^{13}C$ records from time periods when atmospheric pCO_2 was much higher than today, or when it underwent rapid changes. For example, proxy reconstructions of pCO_2 during the Eocene (57 to 32 Myr ago) range between 500 and more than 1000 µatm. Such high pCO_2 would have had a first-order effect on the distribution of $\delta^{13}C$ in the ocean by greatly accelerating equilibration, causing the vertical gradient to weaken, in the absence of other changes. What is more, if pCO_2 increased rapidly during a short interval, it could be expected to have caused a transient collapse in the vertical $\delta^{13}C$ gradient, mimicking an absence of a biological pump, a state which has been termed a Strangelove Ocean [*Hsü and McKenzie*, 1985]. This effect could explain the sharp deviation to a weaker vertical gradient recorded in high-resolution $\delta^{13}C$ records of the Southern Ocean when atmospheric pCO_2 increased during the Paleocene-Eocene Thermal Maximum. In addition, it could provide an alternate explanation for the collapse in the vertical $\delta^{13}C$ at the Cretaceous-Paleogene boundary [*Hsü and McKenzie*, 1985], if a large and rapid increase in pCO_2 eliminated isotopic disequilibrium, rather than a shutdown of biological export. This explanation could potentially reconcile the

$\delta^{13}C$ observations with recently published faunal evidence that refutes a weakening of the biological pump at this time [*Alegret et al.*, 2012], and the resilience of marine upper trophic level organisms across the end Cretaceous extinction event [*Sibert et al.*, 2014].

6. Summary

1. The equilibration timescale of carbon isotope ratios in the surface ocean is directly proportional to the ratio DIC/CO_2. Under low pCO_2, the DIC/CO_2 ratio is large, and the equilibration rate is therefore slow. This simple chemical principle causes pCO_2 to exert a first-order impact on the $\delta^{13}C$ and $\Delta^{14}C$ of the ocean and atmosphere.
2. The pCO_2 effect acts as a modulator of surface ocean disequilibrium. Since the disequilibrium for $\Delta^{14}C$ is due to radioactive decay, while the $\delta^{13}C$ disequilibrium is due to mass-dependent fractionation, the effect is fundamentally different for the two isotopes. For $\Delta^{14}C$, higher pCO_2 causes the ocean to take up ^{14}C more rapidly, lowering the $\Delta^{14}C$ of the atmosphere. For $\delta^{13}C$, higher pCO_2 causes oceanic $\delta^{13}C$ to become a more faithful expression of the thermodynamic and biological signals, which are generally opposite in the modern ocean, so that higher pCO_2 leads to weaker $\delta^{13}C$ gradients in the ocean.
3. During the LGM, the atmospheric $\Delta^{14}C$ would have been >30‰ higher than at present as a result of the pCO_2 effect. This helps to close the gap between the reconstructed high $\Delta^{14}C$ of the glacial atmosphere and the estimated glacial ^{14}C production rate, without requiring any increase of benthic-planktonic ventilation ages. Meanwhile, the atmospheric $\Delta^{14}C$ increase would have caused surface ocean reservoir ages during the LGM to have been approximately 250 years older than today, due to the pCO_2 effect. For most of the low-latitude ocean, a simple linear correction of surface reservoir age versus $1/pCO_2$ approximates this effect well. Variable inputs of ^{14}C-depleted deep waters, such as due to changes in upwelling or vertical mixing, and transient changes in ^{14}C production, would be additive to the pCO_2 effect in determining surface reservoir age changes.
4. During the LGM, all else being equal, the $\delta^{13}C$ of waters ventilated in the Southern Ocean would be expected to have been approximately 0.2‰ lower relative to the atmosphere, upper ocean, and North Atlantic Deep Water, due to the pCO_2 effect. This would have contributed to the strong vertical $\delta^{13}C$ gradients of the LGM, reconstructed from benthic foraminiferal data [e.g., *Sarnthein et al.*, 1994; *Curry and Oppo*, 2005; *Ziegler et al.*, 2013], and to the exceptionally low $\delta^{13}C$ of the deep Southern Ocean [*Ninnemann and Charles*, 2002]. However, it is insufficient to explain the full signal, which must also have included larger changes in $\delta^{13}C$ due to altered ocean circulation and/or the biological pump. Nonetheless, this emphasizes the degree to which $\delta^{13}C$ depends on air-sea exchange, and strongly cautions against its interpretation as a proxy for nutrient concentrations.
5. During the more distant past, such as the early Cenozoic, very high atmospheric pCO_2 could have eliminated much of the carbon isotopic disequilibrium in the ocean. This would have had a first-order effect on benthic foraminiferal $\delta^{13}C$ records. Because disequilibrium causes the deep ocean $\delta^{13}C$ to be low relative to the surface, high pCO_2 would have raised the deep ocean $\delta^{13}C$, mimicking a weak biological pump and/or rapid deep ocean ventilation. Under very high pCO_2, with ocean circulation and the biological pump similar to today, the vertical $\delta^{13}C$ gradient could have been largely eliminated or even reversed.
6. The equilibration timescale for carbon isotopes has decreased by $\approx$ 30% since the preindustrial and will continue to decrease as long fossil fuel combustion continues to raise pCO_2. Although the pCO_2 effect is still overshadowed by the ongoing redistribution of bomb radiocarbon, it will become increasingly evident that radiocarbon is being more rapidly taken up by the ocean as time progresses, driving the atmospheric $\Delta^{14}C$ to lower values. Similarly, the disequilibrium for $\delta^{13}C$ at the ocean surface is currently shrinking, which will gradually weaken $\delta^{13}C$ gradients within the ocean, causing the North Atlantic and Southern Ocean waters to become more isotopically similar. For both isotope systems, the anthropogenic pCO_2 effect tends to be generally in the same sense, and of the same order, as the better known Suess effect.

Appendix A: Derivation of Isotopic Air-Sea Equilibration Timescale

This appendix follows the derivation made by one of us (J. L. S.), which was detailed in an internal university memo in December 1997, but not previously published. It provided the intellectual foundation for this article.

In the absence of other sources or sinks and ignoring mixing with underlying waters, the time evolution of the surface mixed layer concentration of a gas (defined as C) due to exchange with the atmosphere can be approximated by the following time-dependent equation:

$$\frac{\partial C_{\text{ocean}}}{\partial t} = \frac{k_w}{z_{\text{ML}}}(C_{\text{sat}} - C_{\text{ocean}}) \tag{A1}$$

where k_w is the gas exchange coefficient (also known as the piston velocity) and z_{ML} is the thickness of the mixed layer at the surface of the ocean [*Sarmiento and Gruber*, 2006]. $(k_w/z_{\text{ML}})^{-1}$ is therefore the *e*-folding equilibration time scale with which the mixed layer concentration C_{ocean} will approach the saturation concentration that would be in equilibrium with the atmosphere, C_{sat}.

For C = DIC (dissolved inorganic carbon), the gas exchange is driven by the concentration of dissolved CO_2 gas relative to its saturation concentration in equilibrium with the atmosphere, so that equation (A1) becomes

$$\frac{\partial \text{DIC}}{\partial t} = \frac{k_w}{z_{\text{ML}}}\left(CO_{2\text{sat}} - CO_{2\text{ocean}}\right) \tag{A2}$$

This is different than the relationship found for other gases which do not react with seawater, since the air-sea flux is driven by a particular species of the dissolved carbon, rather than by its total concentration. Thus, the equilibration timescale for DIC will be determined by the equilibration timescale of dissolved CO_2. We can gain insight into this by expanding the time rate of change of DIC as

$$\frac{\partial \text{DIC}}{\partial t} = \frac{\partial \text{DIC}}{\partial \text{CO}_{2\text{ocean}}} \cdot \frac{\partial \text{CO}_{2\text{ocean}}}{\partial t} \tag{A3}$$

and rearranging to solve for the time rate of change of CO_2,

$$\frac{\partial \text{CO}_{2\text{ocean}}}{\partial t} = \left(\frac{\partial \text{DIC}}{\partial \text{CO}_{2\text{ocean}}}\right)^{-1} \frac{k_w}{z_{\text{ML}}}(\text{CO}_{\text{sat}} - \text{CO}_{2\text{ocean}}) \tag{A4}$$

Thus, the *e*-folding equilibration time scale for $CO_{2\text{ocean}}$, and therefore, DIC in the mixed layer is

$$\tau_{\text{DIC}} = \left(\frac{\partial \text{DIC}}{\partial \text{CO}_{2\text{ocean}}}\right) \cdot \frac{k_w}{z_{\text{ML}}}^{-1} \tag{A5}$$

This shows that the timescale for the overall equilibration of DIC is set by the buffer capacity, $\delta\text{DIC}/\delta\text{CO}_{2\text{ocean}}$.

Since all isotopes of carbon obey the same chemistry, we can write

$$\frac{\partial \text{DI}^{12}\text{C}}{\partial t} = \frac{k_w}{z_{\text{ML}}}\left({}^{12}CO_{2\text{sat}} - {}^{12}\,\text{CO}_{2\text{ocean}}\right) \tag{A6}$$

$$\frac{\partial \text{DI}^{13}\text{C}}{\partial t} = \frac{k_w}{z_{\text{ML}}}\left({}^{13}\text{CO}_{2\text{sat}} - {}^{13}\,\text{CO}_{2\text{ocean}}\right) \tag{A7}$$

Furthermore, because the speciation of carbon between CO_2, H_2CO_3, HCO_3^-, and CO_3^{2-} is determined by the overall chemical environment, which is itself dependent on the total DIC (including all isotopes), we can write

$$\frac{\text{DIC}}{\text{CO}_{2\text{ocean}}} = \frac{\text{DI}^{12}\text{C}}{{}^{12}\text{CO}_{2\text{ocean}}} = \frac{\text{DI}^{13}\text{C}}{{}^{13}\text{CO}_{2\text{ocean}}} \tag{A8}$$

Note that for brevity, we will treat only ^{13}C and its ratio to ^{12}C here, though the equations for ^{14}C are exactly equivalent.

Ignoring the relatively small mass-dependent isotopic fractionation between species, which is on the order of 1% [*Zeebe and Wolf-Gladrow*, 2001], we obtain the following approximations,

$$\text{DI}^{12}\text{C} = \frac{\text{DIC}}{\text{CO}_{2\text{ocean}}} \cdot {}^{12}\text{CO}_{2\text{ocean}} \tag{A9}$$

$$DI^{13}C = \frac{DIC}{CO_{2ocean}} \cdot {}^{13}CO_{2ocean} \tag{A10}$$

For the purposes of the current work, we would like to know the time derivative of an isotopic ratio for dissolved inorganic carbon, such as $^{13}C/^{12}C$. We start the derivation with a chain rule expansion of the time derivative,

$$\frac{\partial}{\partial t}\left(\frac{DI^{13}C}{DI^{12}C}\right) = \frac{1}{(DI^{12}C)^2}\left(\frac{\partial DI^{13}C}{\partial t} \cdot DI^{12}C - \frac{\partial DI^{12}C}{\partial t} \cdot DI^{13}C\right) \tag{A11}$$

Substituting and rearranging leads to

$$\frac{\partial}{\partial t}\left(\frac{DI^{13}C}{DI^{12}C}\right) = \frac{DI^{13}C}{(DI^{12}C)}\left(\frac{DIC}{CO_{2ocean}}\right)^{-1}\left(\frac{{}^{12}CO_{2sat}}{{}^{13}CO_{2ocean}}\right)\frac{k_w}{z_{ML}}\left(\frac{{}^{13}CO_{2sat}}{{}^{12}CO_{2sat}} - \frac{{}^{13}CO_{2ocean}}{{}^{12}CO_{2ocean}}\right) \tag{A12}$$

This shows that the timescale of equilibration for the isotope ratio is similar to the standard gas exchange formulation but including an additional multiplicative term,

$$\frac{DI^{13}C}{DI^{12}C}\left(\frac{DIC}{CO_{2ocean}}\right)^{-1}\left(\frac{{}^{12}CO_{2sat}}{{}^{13}CO_{2ocean}}\right) \tag{A13}$$

Given the equality of equation (A8), we can simplify the multiplicative term to

$$\frac{{}^{12}CO_{2sat}}{DI^{12}C} \tag{A14}$$

Again, using equation (A8) and taking the assumption that the ocean and atmosphere remain at a relatively consistent degree of equilibration with respect to pCO_2, we see that the equilibration time for the isotope ratio does not vary with the buffer capacity but rather on the ratio of DIC to CO_2:

$$\tau_{DI^{13}C/DI^{12}C} = \tau_{\delta DIC} = \frac{DIC}{CO_{2ocean}} \cdot \left(\frac{k_w}{z_{ML}}\right)^{-1} \tag{A15}$$

Acknowledgments
All model output is available from Eric Galbraith at eric.galbraith@mcgill.ca. E.D.G. and D.B. were supported by the Canadian Institute For Advanced Research (CIFAR) and the Natural Sciences and Engineering Research Council of Canada (NSERC). E.Y.K. was supported by award NRF-2013R1A1A1058203 from the National Research Foundation of Korea. M.P.H. was supported by United Kingdom NERC grant NE/K00901X/1. This work was supported by the Carbon Mitigation Initiative (CMI) project at Princeton University, sponsored by B.P. We thank Mick Follows and Taka Ito for helpful discussions. Andy Ridgwell and one anonymous reviewer provided extremely constructive and insightful reviews.

References

Alegret, L., E. Thomas, and K. C. Lohmann (2012), End-Cretaceous marine mass extinction not caused by productivity collapse, *Proc. Natl. Acad. Sci.*, *109*(3), 728–732.

Bard, E. (1998), Geochemical and geophysical implications of the radiocarbon calibration, *Geochim. Cosmochim. Acta*, *62*(12), 2025–2038, doi:10.1016/S0016-7037(98)00130-6.

Beer, J., U. Siegenthaler, G. Bonani, R. Finkel, H. Oeschger, M. Suter, and W. Wolfli (1988), Information on past solar activity and geomagnetism from ^{10}Be in the Camp Century ice core, *Nature*, *331*(6158), 675–679.

Broecker, W., and S. Barker (2007), A 190 permil drop in atmosphere's delta 14-C during the "Mystery Interval" (17.5 to 14.5 kyr), *Earth Planet. Sci. Lett.*, *256*, 90–99.

Broecker, W., E. Clark, and S. Barker (2008), Near constancy of the Pacific Ocean surface to mid-depth radiocarbon-age difference over the last 20 kyr, *Earth Planet. Sci. Lett.*, *274*(3–4), 322–326, doi:10.1016/J.Epsl.2008.07.035.

Broecker, W. S., and E. Maier-Reimer (1992), The influence of air and sea exchange on the carbon isotope distribution in the sea, *Global Biogeochem. Cycles*, *6*(3), 315–320.

Broecker, W. S., and T. H. Peng (1974), Gas-exchange rates between air and sea, *Tellus*, *26*(1–2), 21–35.

Burke, A., and L. F. Robinson (2012), The Southern Ocean's role in carbon exchange during the last deglaciation, *Science*, *335*(6068), 557–561.

Burkhardt, S., U. Riebesell, and I. Zondervan (1999), Effects of growth rate, CO_2 concentration, and cell size on the stable carbon isotope fractionation in marine phytoplankton, *Geochim. Cosmochim. Acta*, *63*(22), 3729–3741.

Butzin, M., M. Prange, and G. Lohmann (2012), Readjustment of glacial radiocarbon chronologies by self-consistent three-dimensional ocean circulation modeling, *Earth Planet. Sci. Lett.*, *317*, 177–184.

Curry, W. B., and D. Oppo (2005), Glacial water mass geometry and the distribution of $\delta^{13}C$ of sigma-CO_2 in the western Atlantic Ocean, *Paleoceanography*, *20*, PA1017, doi:10.1029/2004PA001021.

de Boyer Montegut, C., G. Madec, A. S. Fischer, A. Lazar, and D. Iudicone (2004), Mixed layer depth over the global ocean: An examination of profile data and a profile-based climatology, *J. Geophys. Res.*, *109*, C12003, doi:10.1029/2004JC002378.

Follows, M., and J. Marshall (1996), On models of bomb 14C in the North Atlantic, *J. Geophys. Res.*, *101*(C10), 22,577–22,582.

Franke, J., A. Paul, and M. Schulz (2008), Modeling variations of marine reservoir ages during the last 45 000 years, *Clim. Past*, *4*(2), 125–136.

Galbraith, E. D., S. L. Jaccard, T. F. Pedersen, D. M. Sigman, G. H. Haug, M. Cook, J. R. Southon, and R. Francois (2007), Carbon dioxide release from the North Pacific abyss during the last deglaciation, *Nature*, *449*(7164), 890–893, doi:10.1038/nature06227.

Hain, M. P., D. M. Sigman, and G. H. Haug (2010), Carbon dioxide effects of Antarctic stratification, North Atlantic Intermediate Water formation, and subantarctic nutrient drawdown during the last ice age: Diagnosis and synthesis in a geochemical box model, *Global Biogeochem. Cycles*, *24*, GB4023, doi:10.1029/2010GB003790.

Hain, M. P., D. M. Sigman, and G. H. Haug (2011), Shortcomings of the isolated abyssal reservoir model for deglacial radiocarbon changes in the mid-depth indo-Pacific Ocean, *Geophys. Res. Lett.*, *38*, L04604, doi:10.1029/2010GL046158.

Hain, M. P., D. M. Sigman, and G. H. Haug (2014), Distinct roles of the Southern Ocean and North Atlantic in the deglacial atmospheric radiocarbon decline, *Earth Planet. Sci. Lett.*, *394*, 198–208.

Hsü, K. J., and J. A. McKenzie (1985), A "Strangelove" ocean in the earliest tertiary, in *The Carbon Cycle and Atmospheric CO_2: Natural Variations Archean to Present, Geophys. Monogr. Ser.*, vol. 32, pp. 487–492, AGU, Washington, D. C.

Hughen, K., S. Lehman, J. Southon, J. Overpeck, O. Marchal, C. Herring, and J. Turnbull (2004), C-14 activity and global carbon cycle changes over the past 50,000 years, *Science*, *303*(5655), 202–207.

Huiskamp, W. N., and K. J. Meissner (2012), Oceanic carbon and water masses during the mystery interval: A model-data comparison study, *Paleoceanography*, *27*, PA4206, doi:10.1029/2012PA002368.

Jones, D. C., T. Ito, Y. Takano, and W. C. Hsu (2014), Spatial and seasonal variability of the air-sea equilibration timescale of carbon dioxide, *Global Biogeochem. Cycles*, *28*(11), 1163–1178, doi:10.1002/2014GB004813.

Key, R. M., A. Kozyr, C. L. Sabine, K. Lee, R. Wanninkhof, J. L. Bullister, R. A. Feely, F. J. Millero, C. Mordy, and T. H. Peng (2004), A global ocean carbon climatology: Results from Global Data Analysis Project (GLODAP), *Global Biogeochem. Cycles*, *18*, GB4031, doi:10.1029/2004GB002247.

Kohler, P., R. Muscheler, and H. Fischer (2006), A model-based interpretation of low-frequency changes in the carbon cycle during the last 120,000 years and its implications for the reconstruction of atmospheric $\Delta^{14}C$, *Geochem. Geophys. Geosyst.*, *7*, Q11N06, doi:10.1029/2005GC001228.

Kwon, E. Y., and F. Primeau (2008), Optimization and sensitivity of a global biogeochemistry ocean model using combined in situ DIC, alkalinity, and phosphate data, *J. Geophys. Res.*, *113*, C08011, doi:10.1029/2007JC004520.

Laj, C., C. Kissel, and J. Beer (2004), High resolution global paleointensity stack since 75 kyr (GLOPIS-75) calibrated to absolute values, in *Timescales of the Paleomagnetic Field*, vol. 145, edited by J. E. T. Channell et al., pp. 255–265, AGU, Washington, D. C.

Lund, D. C., A. C. Mix, and J. Southon (2011), Increased ventilation age of the deep northeast Pacific Ocean during the last deglaciation, *Nat. Geosci.*, *4*(11), 771–774, doi:10.1038/ngeo1272.

Lynch-Stieglitz, J., T. F. Stocker, W. S. Broecker, and R. G. Fairbanks (1995), The influence of air-sea exchange on the isotopic composition of oceanic carbon—Observations and modeling, *Global Biogeochem. Cycles*, *9*(4), 653–665.

Mook, W. G., J. C. Bommerso, and W. H. Staverma (1974), Carbon isotope fractionation between dissolved bicarbonate and gaseous carbon-dioxide, *Earth Planet. Sci. Lett.*, *22*(2), 169–176.

Müller, S., F. Joos, G.-K. Plattner, N. Edwards, and T. Stocker (2008), Modeled natural and excess radiocarbon: Sensitivities to the gas exchange formulation and ocean transport strength, *Global Biogeochem. Cycles*, *22*, GB3011, doi:10.1029/2007GB003065.

Murnane, R., and J. Sarmiento (2000), Roles of biology and gas exchange in determining the $\delta^{13}C$ distribution in the ocean and the preindustrial gradient in atmospheric $\delta^{13}C$, *Global Biogeochem. Cycles*, *14*(1), 389–405, doi:10.1029/1998GB001071.

Murnane, R., J. L. Sarmiento, and C. Le Quéré (1999), Spatial distribution of air-sea CO_2 fluxes and the interhemispheric transport of carbon by the oceans, *Global Biogeochem. Cycles*, *13*(2), 287–305.

Muscheler, R., J. Beer, G. Wagner, C. Laj, C. Kissel, G. M. Raisbeck, F. Yiou, and P. W. Kubik (2004), Changes in the carbon cycle during the last deglaciation as indicated by the comparison of Be-10 and C-14 records, *Earth Planet. Sci. Lett.*, *219*(3–4), 325–340.

Naegler, T., P. Ciais, K. Rodgers, and I. Levin (2006), Excess radiocarbon constraints on air-sea gas exchange and the uptake of CO_2 by the oceans, *Geophys. Res. Lett.*, *33*, L11802, doi:10.1029/2005GL025408.

Najjar, R. G., et al. (2007), Impact of circulation on export production, dissolved organic matter, and dissolved oxygen in the ocean: Results from phase II of the Ocean Carbon-Cycle Model Intercomparison Project (OCMIP-2), *Global Biogeochem. Cycles*, *21*, GB3007, doi:10.1029/2006GB002857.

Ninnemann, U. S., and C. D. Charles (2002), Changes in the mode of southern ocean circulation over the Last Glacial Cycle revealed by foraminiferal stable isotopic variability, *Earth Planet. Sci. Lett.*, *201*(2), 383–396.

Popp, B. N., R. Takigiku, J. M. Hayes, J. W. Louda, and E. W. Baker (1989), The post-Paleozoic chronology and mechanism of ^{13}C depletion in primary marine organic matter, *Am. J. Sci.*, *289*, 436–454.

Primeau, F. (2005), Characterizing transport between the surface mixed layer and the ocean interior with a forward and adjoint global ocean transport model, *J. Phys. Oceanogr.*, *35*(4), 545–564.

Ramsey, C. B., et al. (2012), A complete terrestrial radiocarbon record for 11.2 to 52.8 kyr BP, *Science*, *338*(6105), 370–374.

Rau, G. H., T. Takahashi, and D. J. D. Marais (1989), Latitudinal variations in plankton $\delta^{13}C$: Implications for CO_2 and productivity in past oceans, *Nature*, *341*(6242), 516–518.

Reimer, P. J., et al. (2004), IntCal04 terrestrial radiocarbon age calibration, 0–26 cal kyr BP, *Radiocarbon*, *46*(3), 1029–1058.

Reimer, P. J., E. Bard, A. Bayliss, J. W. Beck, P. G. Blackwell, C. B. Ramsey, C. E. Buck, H. Cheng, R. L. Edwards, and M. Friedrich (2013), $IntCal_{13}$ and $Marine_{13}$ radiocarbon age calibration curves 0–50,000 years cal BP, *Radiocarbon*, *55*(4), 1869–1887.

Sarmiento, J., and N. Gruber (2006), *Ocean Biogeochemical Dynamics*, Princeton Univ. Press, Princeton and Oxford, U. K.

Sarnthein, M., K. Winn, S. J. Jung, J. Duplessy, L. Labeyrie, H. Erlenkeuser, and G. Ganssen (1994), Changes in east Atlantic deepwater circulation over the last 30,000 years: Eight time slice reconstructions, *Paleoceanography*, *9*(2), 209–267.

Sarnthein, M., M. Grootes, J. P. Kennett, and M.-J. Nadeau (2007), ^{14}C reservoir ages show deglacial changes in ocean currents and carbon cycle, in *Past and future changes of the Oceanic Meridional Overturning Circulation: Mechanisms and Impacts, Geophys. Monogr. Ser.*, edited by A. Schmittner, J. C. H. Chiang, and S. R. Hemming, pp. 175–196, AGU, Washington, D. C.

Schmittner, A. (2003), Southern Ocean sea ice and radiocarbon ages of glacial bottom waters, *Earth Planet. Sci. Lett.*, *213*(1–2), 53–62.

Schmittner, A., N. Gruber, A. Mix, R. Key, A. Tagliabue, and T. Westberry (2013), Biology and air–sea gas exchange controls on the distribution of carbon isotope ratios ($\delta^{13}C$) in the ocean, *Biogeosci. Discuss.*, *10*(5), 8415–8466.

Sibert, E. C., P. M. Hull, and R. D. Norris (2014), Resilience of pacific pelagic fish across the cretaceous/palaeogene mass extinction, *Nat. Geosci.*, *7*(9), 667–670.

Siegenthaler, U. (1986), Carbon dioxide: Its natural cycle and anthropogenic perturbation, in *The Role of Air-Sea Exchange in Geochemical Cycling*, edited by U. Siegenthaler, pp. 209–247, D. Reidel, Netherlands.

Skinner, L. C., S. Fallon, C. Waelbroeck, E. Michel, and S. Barker (2010), Ventilation of the deep Southern Ocean and deglacial CO_2 rise, *Science*, *328*(5982), 1147–1151, doi:10.1126/science.1183627.

Southon, J., A. L. Noronha, H. Cheng, R. L. Edwards, and Y. Wang (2012), A high-resolution record of atmospheric ^{14}C based on Hulu cave speleothem H82, *Quat. Sci. Rev.*, *33*, 32–41, doi:10.1016/j.quascirev.2011.11.022.

Stocker, T. F., and D. G. Wright (1996), Rapid changes in ocean circulation and atmospheric radiocarbon, *Paleoceanography*, *11*(6), 773–795.
Stuiver, M., and H. Polach (1977), Reporting of ^{14}C data, *Radiocarbon*, *19*, 355–363.
Tans, P., A. De Jong, and W. Mook (1979), Natural atmospheric ^{14}C variation and the Suess effect, *Nature*, *280*, 826–828.
Wanninkhof, R. (1992), Relationship between wind-speed and gas-exchange over the ocean, *J. Geophys. Res.*, *97*(C5), 7373–7382.
Young, J., J. Bruggeman, R. Rickaby, J. Erez, and M. Conte (2013), Evidence for changes in carbon isotopic fractionation by phytoplankton between 1960 and 2010, *Global Biogeochem. Cycles*, *27*(2), 505–515, doi:10.1002/gbc.20045.
Zeebe, R. E., and D. Wolf-Gladrow (2001), *CO_2 in Seawater: Equilibrium, Kinetics, Isotopes: Equilibrium, Kinetics, Isotopes*, Elsevier, New York.
Zhang, J., P. D. Quay, and D. O. Wilbur (1995), Carbon-isotope fractionation during gas-water exchange and dissolution of CO_2, *Geochim. Cosmochim. Acta*, *59*(1), 107–114.
Ziegler, M., P. Diz, I. R. Hall, and R. Zahn (2013), Millennial-scale changes in atmospheric CO_2 levels linked to the southern ocean carbon isotope gradient and dust flux, *Nat. Geosci.*, *6*(6), 457–461.

Erratum

In the originally published version of this article, there was a minor typographical error in Equation A11. This error has been corrected, and this version may be considered the authoritative version of record.